Thermal buckling transition in graphene: Static and dynamical critical exponents

Enzo Granato [1], K. R. Elder [2], S. C. Ying [3], and T. Ala-Nissila [4,5]

[1] *Instituto Nacional de Pesquisas Espaciais, 12227-010 São José dos Campos, SP, Brazil*

[2] *Department of Physics, Oakland University, Rochester, Michigan 48309, USA*

[3] *Department of Physics, P.O. Box 1843, Brown University, Providence, Rhode Island 02912-1843, USA*

[4] *QTF Centre of Excellence, Department of Applied Physics, Aalto University, P.O. Box 15600, FI-00076 Aalto, Espoo, Finland*

[5] *Interdisciplinary Centre for Mathematical Modelling, Department of Mathematical Sciences, Loughborough University, Loughborough, Leicestershire LE11 3TU, United Kingdom*

(Received 16 June 2024; revised 21 October 2024; accepted 17 December 2024; published 6 January 2025)

We study numerically the thermal buckling transition in graphene membranes under compressive strain and clamped boundaries employing an atomistic quasiharmonic model. The numerical simulations combine three different Monte Carlo methods, local moves, collective wave moves and parallel tempering. We determine the static and the dynamical critical exponents by finite-size scaling, and the nonlinear response to a transverse force near the transition. The correlation length exponent and the nonlinear response are in good agreement with recent renormalization-group calculations of elastic membranes. Despite the applied strain, we find a dynamical critical exponent and diffusion exponent of height fluctuations at the transition close to the value for freestanding graphene, $z = 2(1 + \zeta)$ and $\alpha = \zeta/(\zeta + 1)$, where ζ is the static roughening exponent, as obtained in a recent study with a phase-field crystal model.

DOI: 10.1103/PhysRevB.111.014102

I. INTRODUCTION

The effects of thermally induced fluctuations in two-dimensional (2D) crystals, such as graphene, have attracted great interest as they have strong influence on the mechanical properties. The understanding of these phenomena can contribute to the discovery of new universality classes in material science and are particularly important for technological applications in nanoelectromechanical devices [1–5]. They allow for a thermally rippled phase observed experimentally in free-standing graphene [6–8], with a bending rigidity and elastic modulus strongly dependent on the length scale [9–11]. They also determine the dynamical behavior, as shown experimentally with scanning tunneling microscopy [12], leading to an anomalous subdiffusive behavior of the height fluctuations, which can be related to the length-scale dependence of the bending rigidity [13]. An applied compression can induce elastic instabilities in the form of a buckling phase transition, which is also strongly affected by thermal fluctuations [14–19]. Recently, a scaling theory of this buckling transition in thermalized elastic membranes was presented by Shankar and Nelson [15], using a continuum model of elastic membranes and the renormalization-group (RG) method, obtaining static critical exponents in a new universality class and length-dependent bending rigidity. For increasing compression or decreasing temperatures in membranes with clamped boundaries, there is a second-order phase transition from a flat phase, where the average height vanishes to a buckled phase, where the up/down symmetry is spontaneously broken. The membrane then develops a finite nonzero average height, which acts as an order parameter for the transition. A particularly interesting consequence of this critical behavior is that, near the transition in the flat phase, the nonlinear height response for sufficiently small applied force displays power-law behavior with an exponent determined by the critical exponent characterizing the buckling transition, which is significantly different from mean-field theory. This behavior finds support in measurements on graphene membranes with clamped boundaries [5] as argued in Ref. [15] and has also been observed recently in numerical simulations of a phase-field crystal model of graphene [18], which also adopts a continuous description of the lattice system but retains structural information at atomistic length scales. Since the scaling theory assumes a continuum description of the material, it should be of interest to find out to which extent it describes the critical behavior of the thermal buckling transition in an atomistic model of crystalline material, such as graphene. Furthermore, as the main results of the renormalization-group approach for freely suspended elastic membranes have been questioned in very recent numerical calculations that show that the bending rigidity remains independent of length scale [20], despite thermal fluctuations, testing the scaling theory for a graphene membrane under compressive strain is of particularly timeliness.

Although the scaling theory and the values of the static critical exponents [15] can fully describe the time-independent phenomena related to the buckling transition, the dynamics effects require knowledge of the dynamic critical exponent z, which characterizes the divergence of the relaxation time. However, currently its value is not available from scaling theory. A very recent study of compressed nanoribbons at finite temperature by Hanakata *et al.* [19], described by an effective theory of a Brownian particle confined to a nonlinear potential, suggests a dynamic exponent given by the scaling relation $z = 4 - \eta$, where $\eta \approx 0.8$ is the static critical exponent describing the scale dependence of elastic constants. Interestingly enough, this analytical expression for z is the

same as for freestanding graphene, $z = 2(1+\zeta)$, where $\zeta = 1-\eta/2$ is the roughening exponent, as argued in a recent study with a phase-field crystal model of graphene [13], earlier in a model of polymerized membranes [21] and more recently in a model of elastic membranes described by the dynamic Föppl–von Kármán equation [22]. Moreover, the anomalous diffusion exponent of height fluctuations observed experimentally in graphene [12] can be related to this dynamic exponent as [13] $\alpha = \zeta/(\zeta+1)$. It thus appears that, right at the buckling transition, the dynamics of a compressed membrane with clamped boundaries might behave as that of an unstrained one, characterized by the exponents ζ and z satisfying the above scaling relation, a property that could also be observable in other two-dimensional crystalline materials. So far, this has not been demonstrated in numerical simulations of atomistic models of compressed graphene.

To this end, in this work we numerically study the thermal buckling transition in graphene membranes with clamped boundaries employing an atomistic quasiharmonic model introduced by Los *et al.* [8]. The numerical simulations combine three different Monte Carlo (MC) methods, standard local moves, collective wave moves [8] and parallel tempering [23]. We determine the static and dynamical critical exponents by finite-size scaling and the nonlinear response to a transverse force near the transition. In particular, the correlation length exponent and the nonlinear response near the transition are in good agreement with the renormalization-group calculations for the continuum model of elastic membranes [15]. Surprisingly, despite the applied strain, the estimate of the dynamical critical exponent and diffusion exponent of height fluctuations at the transition are close to the value for the unstrained system without clamped boundaries, $z = 2(1+\zeta)$ and $\alpha = \zeta/(\zeta+1)$, depending only on the static critical exponent ζ.

II. QUASIHARMONIC MODEL OF GRAPHENE AND MONTE CARLO SIMULATION

We consider the simple quasiharmonic model of graphene studied by Los *et al.* [8], which is convenient for the MC simulations of the buckling phase transition since it involves only nearest-neighbor interactions with a minimum number of parameters. Inclusion of additional terms with different parameters would provide a more detailed description [24,25]. However, despite its simplicity, the model has already been shown to give results for the scaling behavior of height fluctuations comparable to a more realistic model [8,26] and therefore it is well suited for the study of the critical behavior of the buckling transition. The Hamiltonian is given by [8]

$$H = \frac{1}{2}\sum_i \sum_{j\neq i} \left(K_r (r_{ij} - r_{\rm eq})^2 + K_\theta \sum_{k\neq i,j} (c_{ijk} - c_{\rm eq})^2 \right) - f \sum_i \hat{z}\cdot\vec{r}_i, \quad (1)$$

where the sums are over the nearest neighbors j and k of atom i located at position $\vec{r}_i$. In the second term, $c_{ijk} = \cos(\theta_{ijk})$ and $c_{\rm eq} = \cos(\theta_{\rm eq})$, where θ_{ijk} is the bond angle between ij and ik. The third new term corresponds to the additional energy contribution due to an external force f applied perpendicularly to the membrane xy plane. For graphene, the ground-state equilibrium distance is $r_{\rm eq} = 1.42$ Å and bond angle $\theta_{\rm eq} = 2\pi/3$. The coupling constants are set to $K_r = 22$ eV Å^{-2} and $K_\theta = 4$ eV. These values were determined by matching to the elastic moduli for isotropic and uniaxial compression of a more realistic model of graphene (long-range carbon bond order potential II) [8,26], which gives a bulk modulus $B = 12.52$ eV Å^{-2} and shear modulus $\mu = 9.95$ eV Å^{-2}. As a result, the Young's modulus $Y = 22.18$ eV Å^{-2} and Poisson ratio 0.12. The bending rigidity of the model was obtained in previous MC simulations [8] as $\kappa = 0.4$ eV.

To obtain equilibrium configurations near the transition, where critical slowing down dominates, the numerical simulations were performed for different temperatures simultaneously, combining three different MC methods: (i) standard random local moves of the particles; (ii) collective (wave) moves [8] consisting of a random transverse wavelike displacement of all atoms in the direction perpendicular to the graphene plane and (iii) exchange of replicas at different temperatures according to the parallel tempering method [23]. A combination of the first two methods was already used to demonstrate that the MC simulations of the model of Eq. (1) can reach equilibrium for unstrained graphene. Here, we find that the additional method (iii) significantly decreases the statistical error of average quantities. A single MC step corresponds to attempt to change the position of all the particles according to the methods (i), (ii), and (iii), in succession.

For the study of equilibrium dynamics, the initial equilibrium configurations were taken from those obtained with the three combined MC methods described above. The subsequent time dependence was then obtained from the first method, standard random local moves of the particles, at a fixed temperature, since the other two methods involves collective moves. Since inertial effects are not included in the MC simulation, it corresponds to an overdamped dynamics (model A) [27] with the unit of time corresponding to one standard MC step.

III. SCALING THEORY OF THE THERMAL BUCKLING TRANSITION OF ELASTIC MEMBRANES

A general scaling theory for the buckling transition of elastic membranes has been developed by Shankar and Nelson [15], with the static critical exponents obtained by the renormalization-group method. Here, we briefly summarize the main results for a system described by a height field $h(\vec{r})$, where $\vec{r}$ is the two-dimensional in-plane coordinate, under a fixed compressive strain $\epsilon < \epsilon_c < 0$ and with clamped boundaries, which will be used in the next section for the interpretation of the numerical simulations. The buckling instability threshold ϵ_c at zero temperature vanishes with increasing system size L as $\epsilon_c \propto -1/L^2$. For decreasing temperatures, there is a second-order phase transition from a flat phase with up/down symmetry to a buckled phase, where this symmetry is spontaneously broken and the membrane develops a finite nonzero average height $\langle h\rangle$, where h denotes the spatially averaged height field, which acts as an order parameter for the transition. Close to the transition, the

correlation length ξ diverges as a function of the deviation from the critical point $\Delta T = T - T_c(\epsilon)$ as

$$\xi \propto |\Delta T|^{-\nu}, \tag{2}$$

characterized by the critical exponent ν. Measurable quantities then display power law scaling with different critical exponents. The average height increases below the transition as

$$\langle h \rangle \propto L|\Delta T|^{\beta}, \tag{3}$$

and the height susceptibility $\chi = (\partial\langle h\rangle/\partial f)|_{f=0}$, which measures the response to an external force f applied transversely to the membrane, diverges as

$$\chi \propto L^2|\Delta T|^{-\gamma}, \tag{4}$$

where L is the system size. The height response satisfy the scaling form

$$\langle h \rangle = L\Delta T^{\beta}\Phi^{\pm}(Lf/\Delta T^{\beta+\gamma}), \tag{5}$$

where $\pm$ correspond to temperatures above and below T_c. Right at the transition, the dependence of the average height on the force is nonlinear,

$$\langle h \rangle \propto Lf^{1/\delta}. \tag{6}$$

The explicit dependence on L in these expressions is different from the conventional finite-size scaling form of critical phenomena. The critical exponents satisfy the scaling relations $\gamma = \nu(2-\eta)$, $\gamma = 2\beta$ and $\delta = (\beta+\gamma)/\beta$. The exponent η characterizes the scaling at the transition of the height-correlation function, $\langle |h(q)|^2\rangle \propto 1/q^{4-\eta}$, with wave vector q and local height fluctuations

$$\langle h^2(r)\rangle \propto L^{2\zeta}, \tag{7}$$

with system size, where $\zeta = 1 - \eta/2$. The values of the static critical exponents obtained by the renormalization-group calculations are $\nu = 1.218$, $\beta = 0.718$, $\gamma = 1.436$ and $\delta = 3$, with $\eta = 0.821$ from the self consistent screening approximation [28].

A particularly interesting consequence of this critical behavior is that, above the transition temperature, the linear response for sufficiently small applied force crosses over to a nonlinear regime with two distinct contributions,

$$f = c_1 \frac{1}{L^{4-1/\beta}} \Delta T \langle h\rangle^{3-1/\beta} + c_2 \frac{1}{L^4}\langle h\rangle^3. \tag{8}$$

The cubic contribution of the second term in the above equation is predicted by mean-field theory while the first is a characteristic feature of the membrane under compression with clamped boundaries as predicted by the scaling theory, leading to a power-law behavior $f \propto \langle h\rangle^{1.607}$ in the intermediate nonlinear regime with a distinct exponent, based on the value of β derived from the renormalization-group calculations. This behavior has been observed recently in numerical simulations of a phase-field crystal model of graphene [18]. The numerical simulations of the quasiharmonic model described in the next section provides additional support for this nonlinear behavior.

Although the above scaling theory and the values of the static critical exponents can fully describe the time-independent phenomena related to the buckling transition, the dynamic effects require knowledge of the dynamic critical exponent z, which characterizes the divergence of the relaxation time $\tau \propto \xi^z$ measuring the exponential decay of the height autocorrelation function with time $C(t) \propto e^{-t/\tau}$. At the transition it should increase as a power law, $\tau \propto L^z$, with system size L, according to finite-size scaling. A recent study of compressed nanoribbons [19], suggests the scaling relation $z = 4 - \eta = 2(1+\zeta)$, which is the same as for freestanding graphene [13,21]. In the latter system, the diffusion exponent of height fluctuations can be related to the dynamic exponent as [13] $\alpha = \zeta/(\zeta+1)$ and appears consistent with experimental measurements [12]. In the next section, we provide a numerical estimate of this unknown dynamic critical exponent and the static critical exponents, from numerical simulations of the quasiharmonic model of graphene described in the previous section.

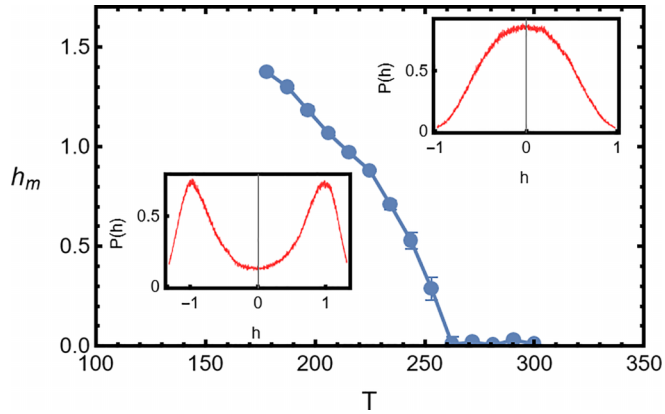

FIG. 1. Temperature dependence of the order parameter (spatial average of the height) h with maximum probability h_m and the height probability distribution $P(h)$ (insets) for temperatures above the transition $T = 272$ (top) and below the transition $T = 216$ (bottom), for a system size $L = 50$ and $\epsilon = -1.2\%$.

IV. NUMERICAL RESULTS

The numerical simulations were performed in systems of dimensionless linear size L ranging from 20 to 80 containing $n = 2L^2$ atoms, corresponding to dimensions $L_x = (1+\epsilon)L(\sqrt{3})r_{eq}$ in the x direction and $L_y = (1+\epsilon)L(\frac{3}{2})r_{eq}$ in the y direction, where $\epsilon < 0$ is the applied strain. Clamped boundary conditions were implemented by fixing two atomic rows or columns of atoms with zero height at the boundaries of the graphene xy plane. The system was first equilibrated at a given temperature with typically 5×10^7 MC steps with equal number of steps to obtain averages. The buckling transition was studied in terms of the height order parameter, defined as the spatial average of the height of the particles $h = \sum_{i=1}^{n} z_i/n$ from the graphene xy plane, where z_i is the z-component of the position vector of the particles (x_i, y_i, z_i). The units of length, force and temperature are Å, eV/Å and K, respectively, while time is measured in MC steps.

Figure 1 shows the temperature dependence of the order parameter with maximum probability h_m and the height probability distribution (inset) for simulations at temperatures well above and below the buckling transition, where

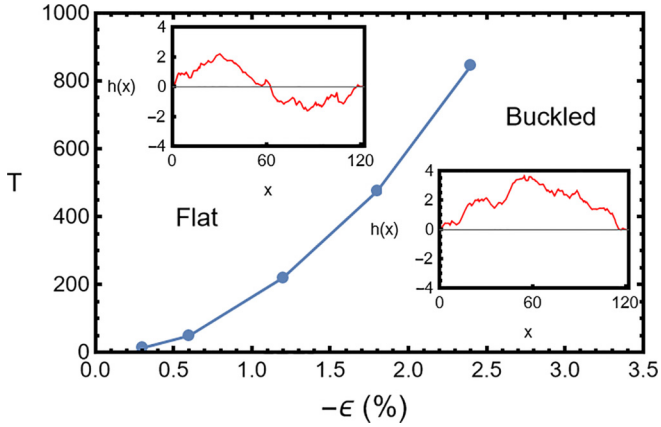

FIG. 2. Phase diagram as function temperature T and compression $\epsilon < 0$ for a system size $L = 50$ and local height configurations $h(x)$ in the x direction at $y = Ly/2$ and $\epsilon = -1.2\%$ (insets) in the flat phase for $T = 281$ (top) and in buckled phase for $T = 159$ (bottom).

$h_{\rm m}$ becomes nonzero. The double-peaked probability distribution with up/down symmetry ($h \to -h$) below the transition demonstrates that the MC simulations properly sample the phase space near the transition. Figure 2 shows the phase diagram as a function of temperature and compression $\epsilon < 0$ for a system size $L = 50$ and the insets illustrate two local height configurations in the x direction, in the flat and buckled phases. The corresponding configurations are shown in Fig. 3. To determine the critical exponents, we performed extensive MC simulations for a fixed value of the compression, $\epsilon = -1.2\%$, as a function of temperature and different system sizes. Additional calculations for a different value of the compression, $\epsilon = -1.8\%$, are presented in Appendix A, giving the same results within the estimated error bars. This is expected since the buckling transition line in the phase diagram of Fig. 2 is controlled by a single fixed point [15].The critical temperature, critical exponents and nonlinear response were obtained from a finite-size scaling analysis as detailed in the following.

A. Static critical exponents

To estimate the critical temperature $T_{\rm c}$ and correlation length exponent ν, we study the temperature and size

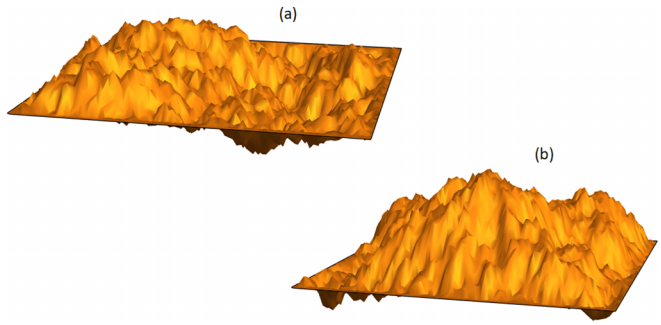

FIG. 3. Height configurations in the flat phase for $T = 281$ (a) and buckled phase for $T = 159$ (b), corresponding to the height profiles in the insets of Fig. 2.

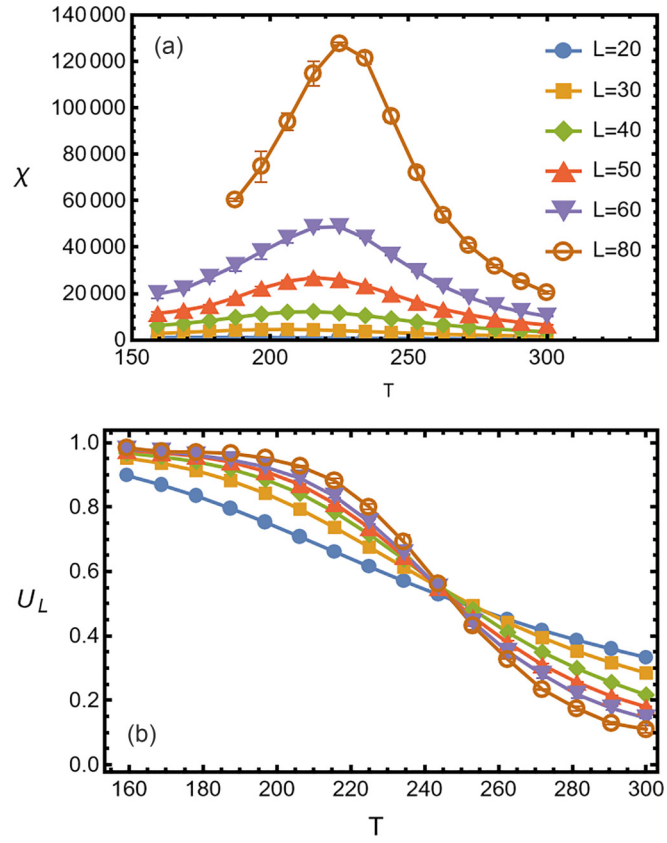

FIG. 4. Temperature dependence of the susceptibility χ (a) and cumulant U_L (b) near the transition for $\epsilon = -1.2\%$ for different system sizes L. Error bars were obtained from three independent runs. When not visible, they are smaller than the symbol sizes.

dependence of the Binder cumulant [29] U_L shown in Fig. 4, defined as

$$U_L(T) = (3 - \langle h^4\rangle/\langle h^2\rangle^2)/2, \tag{9}$$

where $\langle \cdots \rangle$ are obtained by averaging over different configurations obtained during the MC simulations, after the system has been equilibrated. Since this quantity is dimensionless, it should satisfy the finite-size scaling form

$$U_L(T) = \bar{U}((T - T_c)L^{1/\nu}), \tag{10}$$

in terms of a single critical exponent, where $\bar{U}(x)$ is a scaling function with $\bar{U}(0)$ a constant. This scaling form implies that at the transition, $T = T_{\rm c}$, curves of U_L versus temperature for different system sizes L should cross at a common point corresponding to the critical temperature and the splay out of the curves near $T_{\rm c}$ allows a determination of the critical exponent ν. Since the temperature derivative $S = (\partial U_L/\partial T)|_{T_{\rm c}}$ increases with system size as

$$S \propto L^{1/\nu}, \tag{11}$$

an estimate of ν can be obtained from a log-log plot of this quantity against L. Figure 5 shows that the behavior of U_L obtained by numerical simulations without the parallel tempering method leads to an increase of the statistical errors, where data for large systems scatter significantly from a smooth curve with larger error bars, making the determination

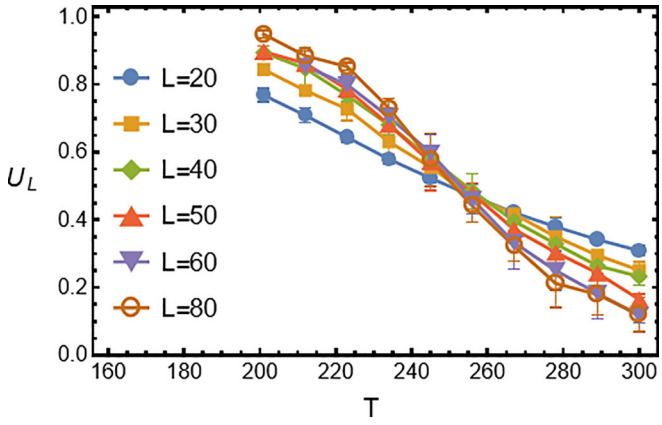

FIG. 5. Cumulant U_L near the transition for $\epsilon = -1.2\%$, obtained by MC simulations without the parallel tempering method.

of the critical temperature from the crossing point and exponent ν less accurate by this method. Therefore, the combination of the three MC methods, local moves, collective wave moves and parallel tempering, described in Sec. II was essential to obtain the results described in the following.

In Fig. 4(b), the curves for U_L versus temperature do not cross precisely at the same point. This is due to statistical errors and corrections to finite-size scaling. The statistical errors arise from the uncertainty of the computed averages, although they are significantly reduced by the present MC method as shown above. Corrections to finite-size scaling arise from the effects of small system sizes, leading to a size dependence of the critical temperature in Eq. (10) and so even data without statistical errors for successive systems would not cross at the same point. However, for $L > 20$ the curves approximately intersect at a common T_c. From the crossing points of pairs of successive system sizes, we obtain slightly different estimates of the critical point. From the average of these values and the mean-square deviations, we obtain a critical temperature and error bar, $T_c = 245(5)$, where it is understood that the number in parentheses is the estimated error in the last digit, $T_c = 245 \pm 5$. Figure 6(a) shows a log-log plot of S evaluated at one of these estimates T_c against L, which gives $\nu = 1.20$ according to Eq. (11). From different estimates of T_c, we obtain $\nu = 1.26(5)$. Sufficiently close to the transition, the data for different temperatures and system sizes should also satisfy the scaling form of Eq. (10). In Fig. 6(b), we show a scaling plot of U_L, obtained by adjusting the parameters T_c and ν to obtain the best data collapse. The scaling function $\bar{U}(x)$ in Eq. (10) is approximated by a Taylor series expansion for small x to fit the data, truncated to low order (fourth to sixth order), which is used as a smooth interpolation function and provide a measure of the data collapse as the least-square residuals [30]. The optimum value is obtained by minimizing the sum of the residuals, leading to the estimates $T_c = 243.5$ and $\nu = 1.275$, which are consistent with the above estimates from the crossing point of $U_L(T)$ and scaling of S.

For the susceptibility critical exponent γ, we explore the temperature and size dependence of the susceptibility shown in Fig. 4, obtained from the height fluctuations as

$$\chi = n(\langle |h|^2 \rangle - \langle |h| \rangle^2)/k_B T. \tag{12}$$

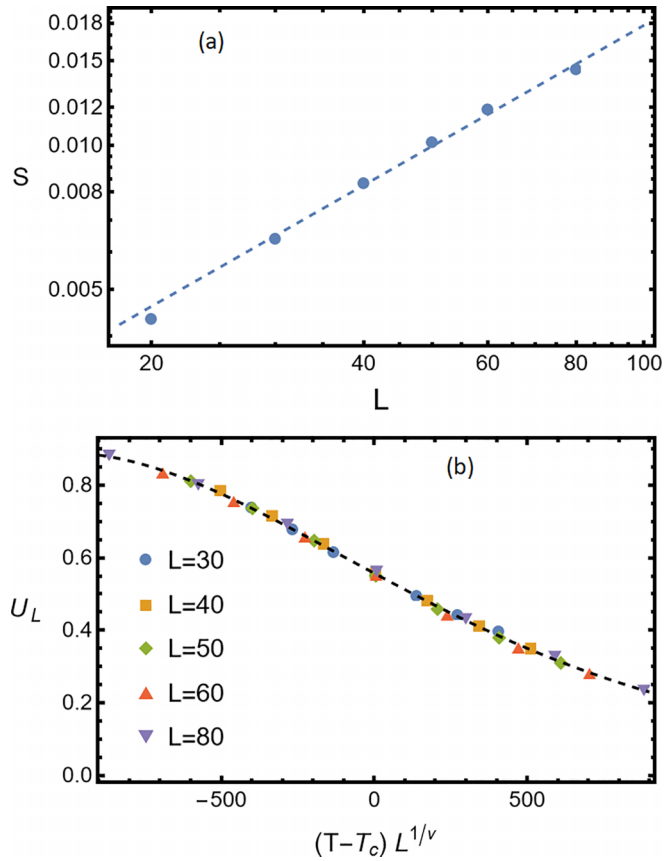

FIG. 6. (a) $S = \partial U_L/\partial T$ at $T = 244.5$ as a function of the system size L. The dotted line is a fit to $L^{1/\nu}$ for $L > 20$ with $\nu = 1.19(4)$. (b) Scaling plot according to Eq. (10) with $T_c = 243.5$ and $\nu = 1.275$.

Although the scaling form of Eq. (4) already contains the system size explicitly, it does not account for the size dependence of the data. To take into account the additional finite-size effects in Eq. (4), we assume that it appears as a scaling function of the dimensionless ratio L/ξ as in conventional finite-size scaling,

$$\chi(T, L) = L^{2+\gamma/\nu} \bar{\chi}((T - T_c)L^{1/\nu}), \tag{13}$$

where $\bar{\chi}(x)$ is another scaling function and $\bar{\chi}(0)$ is a constant. Since at the critical temperature, $\chi(T_c, L) \propto L^{2+\gamma/\nu}$, the ratio γ/ν can be obtained from a log-log plot of this quantity against L. This is shown in Fig. 7(a) at a critical temperature obtained from the crossing point of two successive system sizes in Fig. 4(b). From the slightly different locations of the crossing point, we obtain $\gamma/\nu = 1.40(7)$. Using the estimate of ν described above leads to $\gamma = 1.76(9)$. In Fig. 7(b), we show a scaling plot of $\chi(T, L)$, obtained by adjusting the parameters T_c, ν and γ to obtain the best data collapse. The optimal values of $T_c = 247$, $\nu = 1.2$ and $\gamma = 1.7$ are again consistent with the above estimates.

Our estimate of $\nu = 1.26(5)$ is in good agreement with the results obtained by the RG calculations [15], $\nu = 1.218$ and $\gamma = 1.436$, however our estimate of $\gamma = 1.76(9)$ is significantly higher. This discrepancy could be due to corrections to the finite-size scaling form, which unfortunately cannot

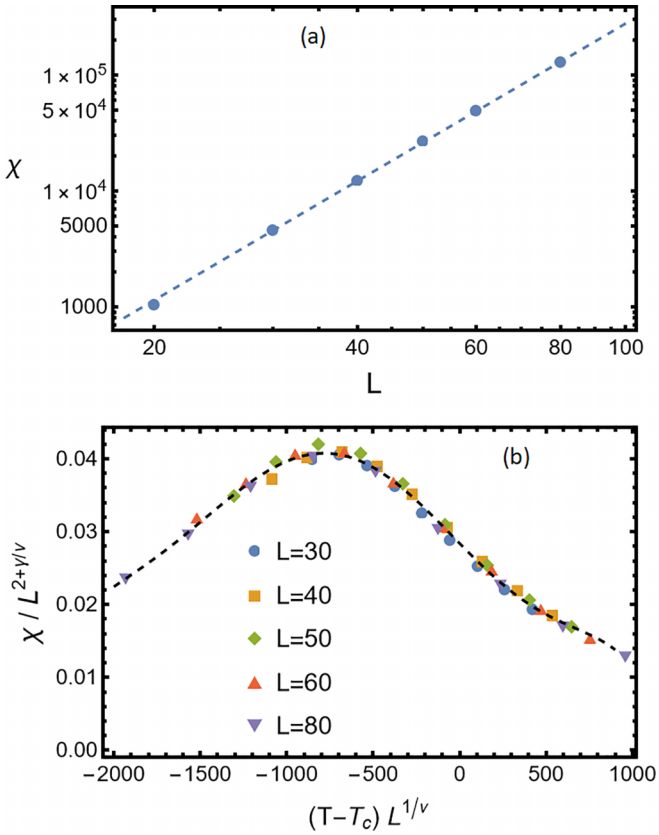

FIG. 7. (a) Susceptibility χ at $T = 244.5$ as a function of system size L. The dotted line is a fit to $L^{2+\gamma/\nu}$ for $L > 20$ with $\gamma/\nu = 1.45(4)$. (b) Scaling plot according to Eq. (13) with $T_c = 247$, $\nu = 1.2$ and $\gamma = 1.7$.

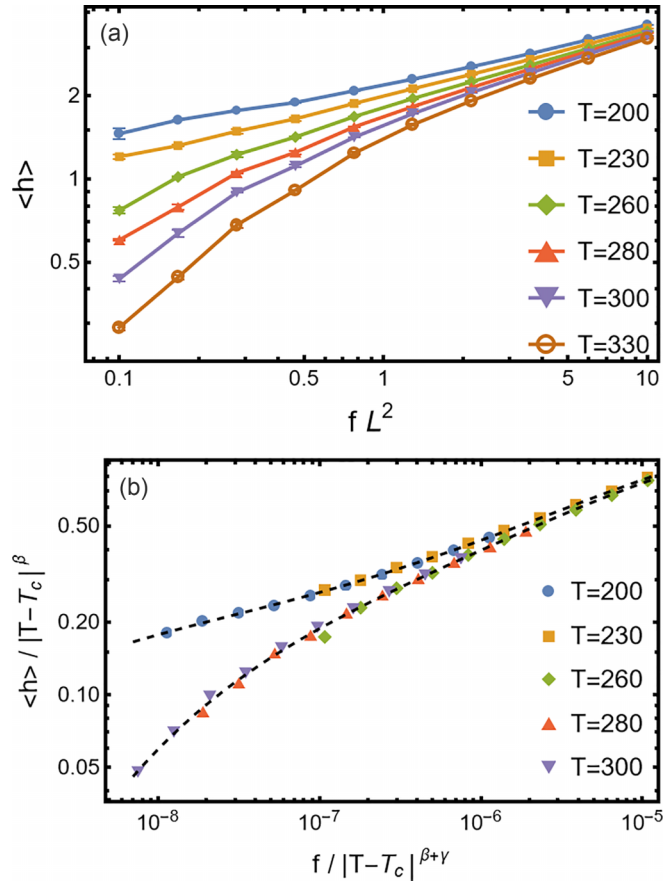

FIG. 8. (a) Height response $\langle h\rangle$ as function of the applied force f for different temperatures T, for $\epsilon = -1.2\%$ and system size $L = 60$. (b) Scaling plot according to Eq. (5) with $T_c = 245$, $\beta = 0.55$ and $\gamma = 1.5$.

be estimated from the present data because of the statistical errors. It is also possible that the systems considered are not sufficiently large for the results of the RG calculations to apply, which is expected to occur when they are much larger than the thermal length [9,15] $L_{\rm th} = \sqrt{16\pi^3\kappa^2/3k_BTY}$. For the quasiharmonic model at the estimated critical temperature, $L_{\rm th} \approx 7$ Å. Although the system sizes used in the present calculations are actually larger than this length scale, this additional correction to scaling could be another reason for the discrepancies in the exponents. Since ν was obtained from the Binder cumulant, which does not have a size dependence outside the scaling form [Eq. (10)], it turns out to be less affected by such systematic errors.

B. Nonlinear response

To study the nonlinear response, we consider the effect of the external force f applied perpendicularly to the graphene xy plane in Eq. (1). Figure 8(a) shows the height response as function of f and temperature for a large system with $L = 60$ and Fig. 8(b) shows the corresponding scaling plot according to Eq. (5), obtained by adjusting the parameters β and γ using the above estimate of T_c. The optimal values of $\beta = 0.55(5)$ and $\gamma = 1.55(5)$ are comparable to the values obtained from the RG calculations [15], $\beta = 0.718$ and $\gamma = 1.436$, although the deviations are outside the estimated error bars. This could be due to finite-size effects, which were neglected to obtain the data collapse.

The behavior of f as a function $\langle h\rangle$ at temperatures above and near the bucking transition is shown in Fig. 9. Above the transition, when the susceptibility is finite and $f = \langle h\rangle/\chi$ for sufficiently small f, there is a crossover from this linear behavior to two different nonlinear behaviors for increasing $\langle h\rangle$. In the intermediate regime, it behaves as a power law, $f \propto \langle h\rangle^a$, with the exponent $a \approx 1.6$, followed by another crossover to $a \approx 3$. Since the range of the linear and intermediate regimes decrease with $T - T_c$, they disappear at the transition and the exponent a corresponds to the critical exponent $\delta = 3$ from Eq. (6). The nonlinear behavior is in good agreement with Eq. (8) predicted by the scaling theory [15] and has also been observed previously in numerical simulations of a phase-crystal model of graphene [18], although using a much smaller systems size.

C. Dynamical exponent

The relaxation time τ relevant for the dynamical behavior can be estimated from the exponential decay at long times t of the height autocorrelation function $C(t) = \langle h(t)h(0)\rangle/\langle h^2\rangle \propto e^{-t/\tau}$, for $T \geqslant T_c$, obtained after the system has reached equilibrium. However, rather than using this time correlation

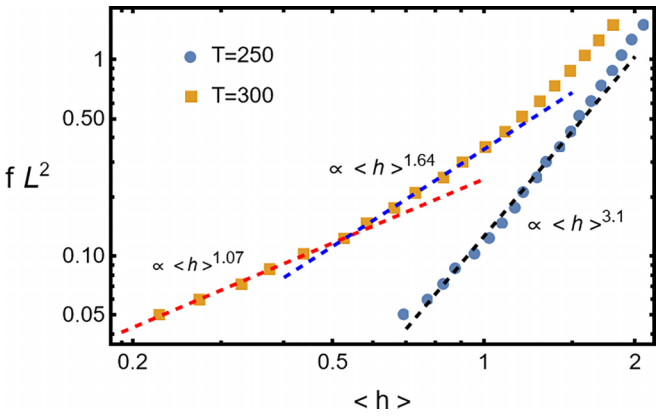

FIG. 9. Applied force f as function of average height $\langle h \rangle$ for different temperatures T near the the buckling transition, for $\epsilon = -1.2\%$ and system size $L = 60$. The dashed lines correspond to power-law behavior $\propto \langle h \rangle^a$. Above the transition, $a = 1.07(4)$ in the range of small f and $a = 1.64(3)$ in the intermediate range, for increasing f. Close to the transition at $T = 250$, $a = 3.1(1)$.

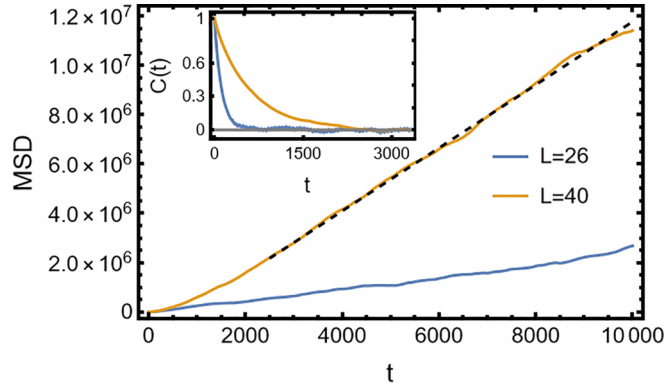

FIG. 10. Normalized mean-squared displacement of $R(t)$, $\text{MSD} = \langle (R(t) - R(0))^2 \rangle / \langle h^2 \rangle$, as a function of MC time t (in units of 2×10^4 MC steps) for different systems sizes at the critical temperature $T_c = 245$ for $\epsilon = -1.2\%$ and corresponding autocorrelation functions (inset). Dashed line indicates linear behavior.

directly, we find it more convenient to obtain τ as a time integral

$$\tau = \frac{1}{\langle h^2 \rangle} \int_0^t dt' \langle h(t')h(0) \rangle, \tag{14}$$

which is formally equivalent to the expression for the diffusion constant of a fictitious particle with coordinate $R(t)$ and velocity $dR(t)/dt = h(t)$. The upper limit of integration in Eq. (14) should be much larger than the relaxation time τ to measure the exponential decay of the autocorrelation function. As in the numerical calculation of diffusion constants [31], it is more accurate to obtain τ from the long time behavior of the mean-squared displacement of $R(t)$ as

$$\tau = \frac{1}{2t \langle h^2 \rangle} \langle (R(t) - R(0))^2 \rangle. \tag{15}$$

To study the time dependence and estimate the dynamic exponent, the initial equilibrium configurations were taken from those obtained with the three combined MC methods described in Sec. II. The subsequent time dependence was then obtained from the first method, standard random local moves of the particles, at a fixed temperature, since the other two methods involves collective moves. Since inertial effects are not included in the MC simulation, it corresponds to an overdamped dynamics. Figure 10 shows the time dependence of $\langle (R(t) - R(0))^2 \rangle / \langle h^2 \rangle$ for different system sizes at the critical temperature and the corresponding autocorrelation functions $C(t)$ in the inset. The linear behavior at long times above a crossover time τ_c of the mean-squared displacement of $R(t)$ demonstrates that the simulation time is sufficiently long and Eq. (15) applies. The estimates of τ obtained from the slopes of the linear fits at long times larger than τ_c are shown in Fig. 11 at the critical temperature and at a higher temperature $T = 300$. The relaxation time increases with system sizes near the transition as expected for a continuous phase transition. Away from the critical temperature in the flat phase, it will eventually reach a finite value, as can be seen from the tendency to saturation at large system sizes for $T = 300$. On the other hand, at the transition it should increase as a power law, $\tau \propto L^z$, according to finite-size scaling, with the dynamic critical exponent z. From a fit to this power law, we then obtain the estimate of $z = 3.64(4)$.

It is interesting to compare our numerical estimate of z from MC simulations with the scaling relation $z = 2(1 + \zeta)$, where $\zeta = 1 - \eta/2$ is the roughening exponent, obtained from other studies. For freestanding graphene, this scaling relation was obtained in a recent study of the dynamical scaling of the mean-squared displacement of the local height $\langle \Delta h(t)^2 \rangle$ with a phase-field crystal model [13] and earlier in a model of polymerized membranes [21]. This quantity displays a subdiffusive behavior determined by the value of z as $\langle \Delta h(t)^2 \rangle \propto t^\alpha$, with $\alpha = \zeta/(1 + \zeta)$, and has been observed experimentally with scanning tunneling microscopy [12]. In the Appendixes, we show results for freestanding graphene, described by the same quasiharmonic model of Eq. (1), which is also well described by the same scaling relation for z. For the buckling transition, using our estimate of $\gamma/\nu = 1.40(7)$ from Sec. IV

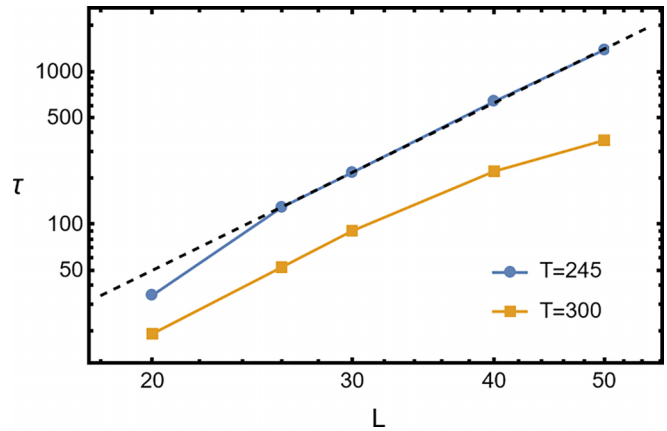

FIG. 11. Relaxation time τ (in units of 2×10^4 MC steps) as a function of system size at and above the critical temperature, $T_c = 245$ and $T = 300$, respectively. Dashed line is a power-law fit to $\tau \propto L^z$ for $L \geqslant 26$, with $z = 3.64(4)$.

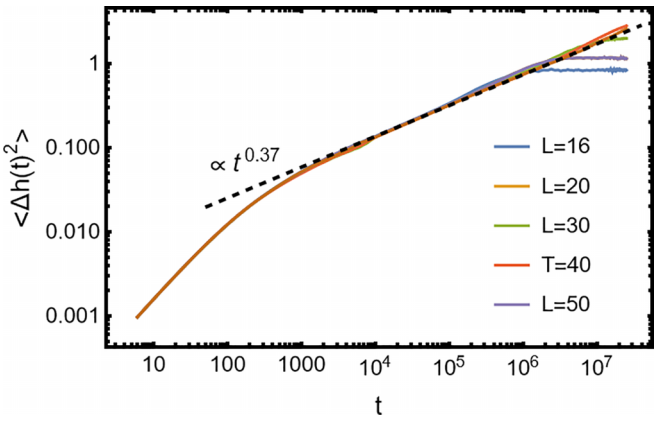

FIG. 12. Mean-squared height displacement $\langle \Delta h(t)^2 \rangle$ of a tagged particle near the center of the graphene membrane as a function of MC time t for different system sizes L at the buckling transition $T_c = 245$ for $\epsilon = -1.2\%$. The dashed line indicates power-law behavior $\langle \Delta h(t)^2 \rangle \propto t^{\alpha}$ in the intermediate time regime with $\alpha = 0.371(1)$ for $L = 50$.

and the scaling relation $\gamma/\nu = 2 - \eta = 2\zeta$ (Sec. III) leads to $z = 2(1+\zeta) = 3.40(7)$, which is very close to the numerical estimate from Fig. 11 at the buckling transition, considering the error bar. It should be noted, however, that using the theoretical value $\eta = 0.821$ from the self-consistent screening approximation [28], gives a larger difference.

It may appear somewhat surprising that the dynamic exponent would be the same as for the freestanding system, since at the buckling transition the system is under compression and with clamped boundaries. However, from the scaling theory of the buckling transition (Sec. III), the average height vanishes and the local height fluctuations scale with system size as $\langle h^2(r) \rangle \propto L^{2\zeta}$ at the critical point, which is the same behavior as for an unstrained membrane without boundary constraints [9,27]. Moreover, the mean-squared height displacement, right at buckling transition, also shows similar subdiffusive behavior as for an unstrained membrane. This is shown in Fig. 12, where the time dependence of $\langle \Delta h(t)^2 \rangle = \langle (z_i(t_0 + t) - z_i(t_0))^2 \rangle$ for a tagged particle i located near center of the membrane is plotted for different system sizes. For larger systems, at intermediate times it behaves as $\langle \Delta h(t)^2 \rangle \propto t^{\alpha}$ with $\alpha = 0.37$, which is consistent with the exponent $\alpha = \zeta/(1+\zeta)$ for freestanding graphene. The main difference is the saturation regime for long times seen for a small system, which is due to the constraint of clamped boundaries, while for the freestanding case it increases linearly with time as shown in the Appendixes. For large systems, the crossover to this regime is beyond the available measurement time.

In a very recent study of the dynamics of the average height in double clamped naroribbons under compression by Hanakata *et al.* [19], the same scaling relation for z was obtained analytically. In the buckled phase, the dynamical transition between opposite buckled states is described by an effective theory of a Brownian particle with damping confined to a double-well potential. The escape time from one the potentials is a measure of the relaxation time of height fluctuations. It was found that it increases with system size as $\tau \sim L^{4-\eta}$, corresponding to a dynamic exponent $z = 2(1+\zeta)$. This relation should be valid in the overdamped limit, which is the case for the dynamics near a continuous buckling transition due to critical fluctuations and in particular for the present MC simulations.

V. SUMMARY AND CONCLUSIONS

In this work, we have studied the thermal buckling transition in graphene membranes with clamped boundaries employing an atomistic quasiharmonic model and MC simulation. We found that the correlation length exponent and the nonlinear response near the transition are in good agreement with the recent RG calculations for the continuum model of elastic membranes [15]. Although the system is under compression and with clamped boundaries, the dynamical critical exponent and the diffusion exponent of height fluctuations at the transition are close to the values for freestanding graphene, $z = 2(1+\zeta)$ and $\alpha = \zeta/(\zeta+1)$. The scaling relation for z has also been obtained in a recent study of compressed nanoribbons [19], described by an effective theory of a Brownian particle confined to a nonlinear potential, in the overdamped limit. The buckling transition can also be induced by an applied stress while the boundary displacements are free to fluctuate. Interestingly, the same scaling theory predicts different critical exponents [15], which could in principle, also be determined by the methods described in this work. Since the critical exponents and the nonlinear response studied here are properties related to the critical point of the buckling transition, it should also be observable in other two-dimensional crystalline materials, besides graphene.

ACKNOWLEDGMENTS

E.G. was supported by the National Council for Scientific and Technological Development-CNPq and computer facilities from the Centro Nacional de Processamento de Alto Desempenho em São Paulo (CENAPAD-SP). K.R.E. would like to acknowledge the support of the National Science Foundation (NSF) under Grant No. DMR-2006456. T.A-N. has been supported in part by the Academy of Finland through its QTF Center of Excellence program Grant No. 312298.

DATA AVAILABILITY

All data shown in the figures are available from the authors upon reasonable request.

APPENDIX A: SCALING ANALYSIS FOR $\epsilon = -1.8\%$ COMPRESSION

Here we briefly describe the results for the static critical exponents obtained at a different value of compression, $\epsilon = -1.8\%$. Figures 13(a) and 13(b) show the behavior of the height susceptibility and Binder cumulant as a function of temperature and system sizes. From the crossing points of pairs of successive system sizes, we obtain a critical temperature $T_c = 543(8)$. Figure 14(a) shows a log-log plot of $S = \partial U_L/\partial T$ evaluated at this estimate of T_c against L, which gives $\nu = 1.20(9)$ according to Eq. (11). From different

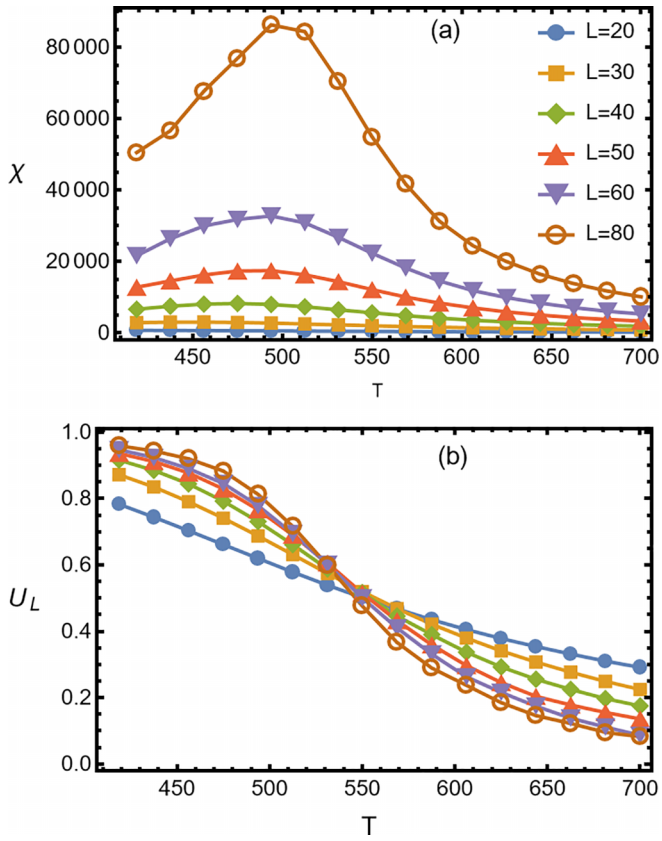

FIG. 13. Temperature dependence of the susceptibility χ (a) and cumulant U_L (b) near the transition for $\epsilon = -1.8\%$ for different system sizes L.

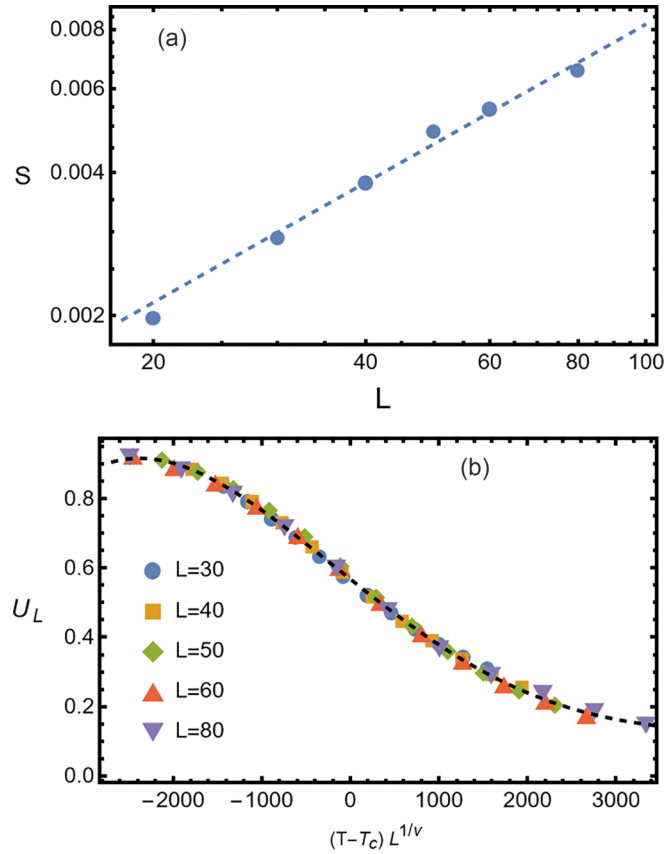

FIG. 14. (a) $S = \partial U_L/\partial T$ at $T = 543$ as a function of the system size L. The dotted line is a fit to $L^{1/\nu}$ for $L > 20$ with $\nu = 1.19(8)$. (b) Scaling plot according to Eq. (10) with $T_c = 243.5$ and $\nu = 1.275$.

estimates of T_c, we obtain $\nu = 1.31(6)$. Sufficiently close to the transition, the data for different temperatures and system sizes should also satisfy the scaling form of Eq. (10). In Fig. 14(b), we show a scaling plot of U_L, obtained by adjusting the parameters T_c and ν to obtain the best data collapse, with optimal values $T_c = 536.4$ and $\nu = 1.275$, which are consistent with the above estimates from the crossing point of $U_L(T)$ and scaling of S.

For the susceptibility critical exponent γ, we explore the temperature and size dependence of the susceptibility shown in Fig. 13. Since at the critical temperature, $\chi(T_c, L) \propto L^{2+\gamma/\nu}$, the ratio γ/ν can be obtained from a log-log plot of this quantity against L. This is shown in Fig. 15(a) at the estimated critical temperature. From the slightly different locations of the crossing point, we obtain $\gamma/\nu = 1.33(7)$. Using the estimate of ν described above leads to $\gamma = 1.75(8)$. In Fig. 7(b), we show a scaling plot of $\chi(T, L)$, obtained by adjusting the parameters T_c, ν and γ to obtain the best data collapse. The optimal values of $T_c = 540$, $\nu = 1.175$ and $\gamma = 1.7$ are consistent with the above estimates.

The estimates of $\nu = 1.31(6)$ and $\gamma = 1.75(8)$ at this value of compression, $\epsilon = -1.8\%$, agrees with the corresponding results for the different value of compression, $\epsilon = -1.2\%$, discussed in the main text. This is expected since the buckling transition line in the phase diagram of Fig. 2 is controlled by a single fixed point, according the RG calculations [15].

APPENDIX B: MEAN-SQUARED HEIGHT DISPLACEMENT FOR FREE-STANDING GRAPHENE

Here we obtain the dynamic exponent z for freestanding graphene, described by the quasiharmonic model of Eq. (1), from the dynamic scaling behavior of the mean-squared height displacement of a tagged particle $\langle \Delta h(t)^2 \rangle = \langle (z(t_0 + t) - z(t_0))^2 \rangle$, where $z(t)$ is the z component of position vector of the tagged particle $(x(t), y(t), z(t))$. The MC simulations were performed without applied compression and with periodic boundary conditions, allowing for fluctuations of the system size in the xy plane. Initial equilibrium configurations were obtained from the first two MC methods described in Sec. II. The subsequent time dependence was then obtained from the first method at a fixed temperature.

Figure 16(a) shows the time dependence of $\langle \Delta h(t)^2 \rangle$ for different systems sizes. For smaller systems, it displays intermediate and long time regimes characterized by a power-law behavior as a function of time. At long times it behaves linearly, which is the conventional diffusive behavior due to the center-of-mass contribution to the height fluctuations. For larger systems, at intermediate times it behaves as $\langle \Delta h(t)^2 \rangle \propto t^\alpha$ with $\alpha < 1$, depending very weakly on system size. For the largest system, the linear behavior is beyond the available measurement time. The crossover from subdiffusive dynamics to normal diffusion at long times and the size dependence can be described by a dynamical scaling theory of equilibrium

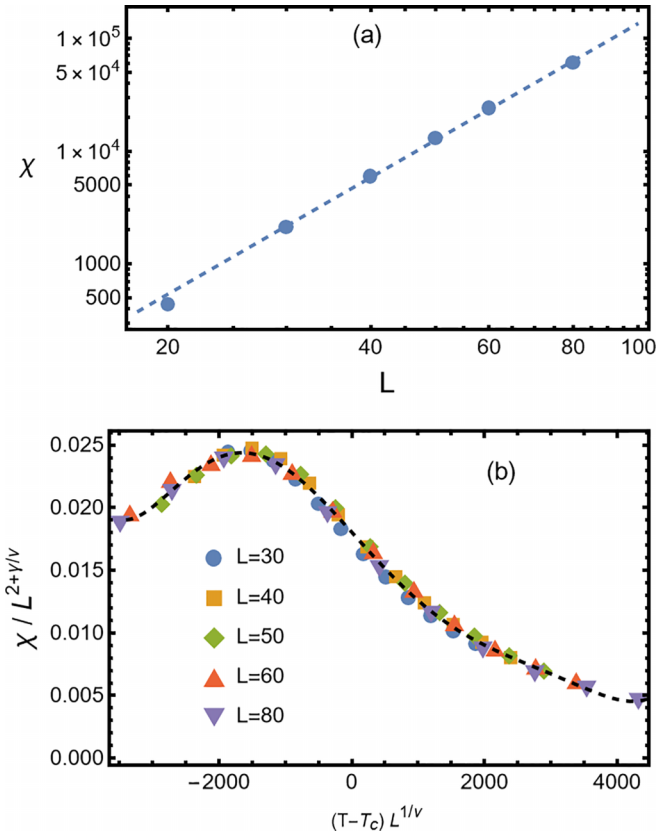

FIG. 15. (a) Susceptibility χ at $T = 543$ as a function of system size L. The dotted line is a fit to $L^{2+\gamma/\nu}$ for $L > 20$ with $\gamma/\nu = 1.43(5)$. (b) Scaling plot according to Eq. (13) with $T_c = 247$, $\nu = 1.2$ and $\gamma = 1.7$.

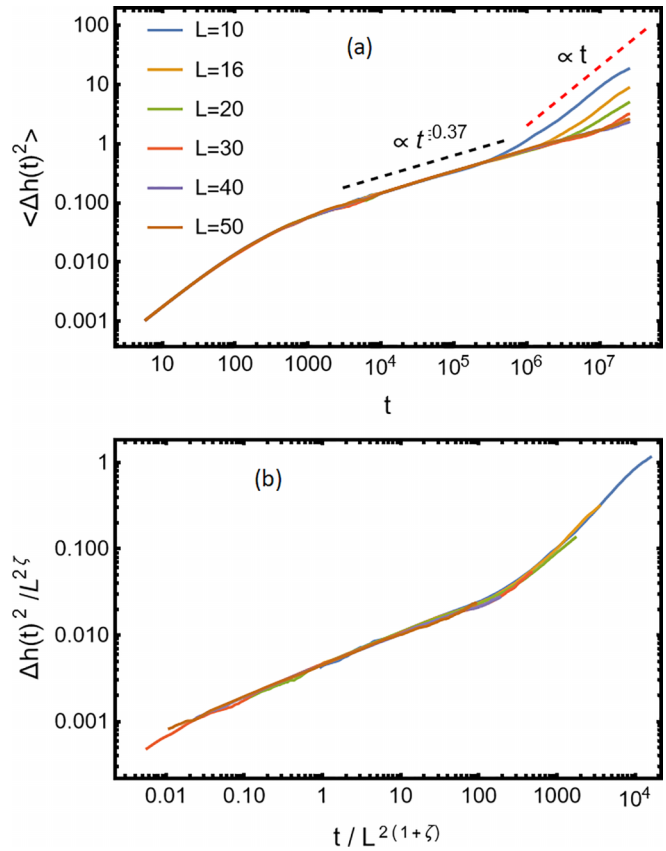

FIG. 16. (a) Mean-squared height displacement $\langle \Delta h(t)^2 \rangle$ for freestanding graphene as a function of MC time t for different system sizes L at a temperature $T = 300$. The black dashed line indicates power-law behavior $\langle \Delta h(t)^2 \rangle \propto t^{\alpha}$ in the intermediate time regime, with $\alpha = 0.371(4)$. The red dashed line indicates the expected linear behavior at long times. (b) Scaling plot for the intermediate and long-time regimes according to Eqs. (B1) and (B2) with $\zeta = 0.6$.

fluctuations [13,21], which assumes the scaling form

$$\langle \Delta h(t)^2 \rangle = L^{2\zeta} \Phi(t/L^z), \tag{B1}$$

where ζ is the roughening exponent [9,27] and

$$z = 2(1 + \zeta), \tag{B2}$$

from the requirement that the contribution from the center-of-mass diffusion in the long-time limit scales as $\langle \Delta h(t)^2 \rangle \sim t/L^2$. In the intermediate-time regime, the scaling function should behave as $\Phi(x) \sim x^{2\zeta/z}$, which implies that $\langle \Delta h(t)^2 \rangle \propto t^{\alpha}$ with $\alpha = \zeta/(1 + \zeta)$.

In Fig. 16(b) we show a scaling plot of $\langle \Delta h(t)^2 \rangle$ vs $t/L^{2(1+\zeta)}$, according to Eq. (B1), adjusting the single parameter ζ. The best data collapse is obtained with the roughening exponent $\zeta = 0.6$. From the scaling relation of Eq. (B2), we then obtain $z = 3.2$, which is comparable to the value for the buckling transition in the same model as described in Sec. IV C. This value of z leads to a mean-squared displacement $\langle \Delta h(t)^2 \rangle \propto t^{\alpha}$ with exponent $\alpha = 0.375$, consistent with the subdiffusive behavior observed experimentally in freestanding graphene with scanning tunneling microscopy [12].

[1] J. S. Bunch, A. M. Van Der Zande, S. S. Verbridge, I. W. Frank, D. M. Tanenbaum, J. M. Parpia, H. G. Craighead, and P. L. McEuen, Electromechanical resonators from graphene sheets, Science **315**, 490 (2007).

[2] P. G. Steeneken, R. J. Dolleman, D. Davidovikj, F. Alijani, and H. S. van der Zant, Dynamics of 2D material membranes, 2D Mater. **8**, 042001 (2021).

[3] P. M. Thibado, P. Kumar, S. Singh, M. Ruiz-Garcia, A. Lasanta, and L. L. Bonilla, Fluctuation-induced current from freestanding graphene, Phys. Rev. E **102**, 042101 (2020).

[4] M. Neek-Amal, P. Xu, J. Schoelz, M. Ackerman, S. Barber, P. Thibado, A. Sadeghi, and F. Peeters, Thermal mirror buckling in freestanding graphene locally controlled by scanning tunnelling microscopy, Nat. Commun. **5**, 4962 (2014).

[5] I. R. Storch, R. De Alba, V. P. Adiga, T. S. Abhilash, R. A. Barton, H. G. Craighead, J. M. Parpia, and P. L. McEuen, Young's modulus and thermal expansion of tensioned graphene membranes, Phys. Rev. B **98**, 085408 (2018).

[6] J. C. Meyer, A. K. Geim, M. I. Katsnelson, K. S. Novoselov, T. J. Booth, and S. Roth, The structure of suspended graphene sheets, Nature (London) **446**, 60 (2007).
[7] A. Fasolino, J. Los, and M. I. Katsnelson, Intrinsic ripples in graphene, Nat. Mater. **6**, 858 (2007).
[8] J. H. Los, M. I. Katsnelson, O. V. Yazyev, K. V. Zakharchenko, and A. Fasolino, Scaling properties of flexible membranes from atomistic simulations: Application to graphene, Phys. Rev. B **80**, 121405(R) (2009).
[9] D. Nelson and L. Peliti, Fluctuations in membranes with crystalline and hexatic order, J. Phys. France **48**, 1085 (1987).
[10] D. Nelson, T. Piran, and S. Weinberg, *Statistical Mechanics of Membranes and Surfaces* (World Scientific, Singapore, 2004).
[11] M. K. Blees, A. W. Barnard, P. A. Rose, S. P. Roberts, K. L. McGill, P. Y. Huang, A. R. Ruyack, J. W. Kevek, B. Kobrin, D. A. Muller *et al.*, Graphene kirigami, Nature (London) **524**, 204 (2015).
[12] M. L. Ackerman, P. Kumar, M. Neek-Amal, P. M. Thibado, F. M. Peeters, and S. Singh, Anomalous dynamical behavior of freestanding graphene membranes, Phys. Rev. Lett. **117**, 126801 (2016).
[13] E. Granato, M. Greb, K. R. Elder, S. C. Ying, and T. Ala-Nissila, Dynamic scaling of out-of-plane fluctuations in freestanding graphene, Phys. Rev. B **105**, L201409 (2022).
[14] E. Guitter, F. David, S. Leibler, and L. Peliti, Crumpling and buckling transitions in polymerized membranes, Phys. Rev. Lett. **61**, 2949 (1988).
[15] S. Shankar and D. R. Nelson, Thermalized buckling of isotropically compressed thin sheets, Phys. Rev. E **104**, 054141 (2021).
[16] A. Morshedifard, M. Ruiz-García, M. J. A. Qomi, and A. Košmrlj, Buckling of thermalized elastic sheets, J. Mech. Phys. Solids **149**, 104296 (2021).
[17] P. Le Doussal and L. Radzihovsky, Thermal buckling transition of crystalline membranes in a field, Phys. Rev. Lett. **127**, 015702 (2021).
[18] E. Granato, K. R. Elder, S. C. Ying, and T. Ala-Nissila, Dynamics of fluctuations and thermal buckling in graphene from a phase-field crystal model, Phys. Rev. B **107**, 035428 (2023).
[19] P. Z. Hanakata, S. S. Bhabesh, D. Yllanes, D. R. Nelson, and M. J. Bowick, Vibrations and transitions across barrier of strained nanoribbons at finite temperature, Phys. Rev. Mater. **8**, 016001 (2024).
[20] U. Aseginolaza, J. Diego, T. Cea, R. Bianco, L. Monacelli, F. Libbi, M. Calandra, A. Bergara, F. Mauri, and I. Errea, Bending rigidity, sound propagation and ripples in flat graphene, Nat. Phys. **20**, 1288 (2024).
[21] K.-I. Mizuochi, H. Nakanishi, and T. Sakaue, Dynamical scaling of polymerized membranes, Europhys. Lett. **107**, 38003 (2014).
[22] C. Steinbock and E. Katzav, Thermally driven elastic membranes are quasi-linear across all scales, J. Phys. A **56**, 215002 (2023).
[23] K. Hukushima and K. Nemoto, Exchange Monte Carlo method and application to spin glass simulations, J. Phys. Soc. Jpn. **65**, 1604 (1996).
[24] A. Lajevardipour, M. Neek-Amal, and F. Peeters, Thermomechanical properties of graphene: Valence force field model approach, J. Phys.: Condens. Matter **24**, 175303 (2012).
[25] V. Perebeinos and J. Tersoff, Valence force model for phonons in graphene and carbon nanotubes, Phys. Rev. B **79**, 241409(R) (2009).
[26] K. V. Zakharchenko, M. I. Katsnelson, and A. Fasolino, Finite temperature lattice properties of graphene beyond the quasiharmonic approximation, Phys. Rev. Lett. **102**, 046808 (2009).
[27] P. Chaikin and T. Lubensky, *Principles of Condensed Matter Physics* (Cambridge University Press, Cambridge, 1995).
[28] P. Le Doussal and L. Radzihovsky, Self-consistent theory of polymerized membranes, Phys. Rev. Lett. **69**, 1209 (1992).
[29] K. Binder, Finite size scaling analysis of Ising model block distribution functions, Z. Phys. B **43**, 119 (1981).
[30] M. P. Nightingale, E. Granato, and J. M. Kosterlitz, Conformal anomaly and critical exponents of the *XY* Ising model, Phys. Rev. B **52**, 7402 (1995).
[31] M. P. Allen and D. J. Tildesley, *Computer Simulation of Liquids* (Oxford University Press, Oxford, 2017).